PA_{63} Channel of Anthrax Toxin: An Extended β-Barrel[†]

Shilla Nassi,[‡] R. John Collier,[§] and Alan Finkelstein*[,‡,||]

Department of Neuroscience and Department of Physiology and Biophysics, Albert Einstein College of Medicine, 1300 Morris Park Avenue, Bronx, New York 10461, and Department of Microbiology and Molecular Genetics, Harvard Medical School, 200 Longwood Avenue, Boston, Massachusetts 02115

Received October 19, 2001; Revised Manuscript Received November 20, 2001

ABSTRACT: Anthrax toxin consists of three protein components: protective antigen (PA), lethal factor (LF), and edema factor (EF). PA_{63}, generated by protease "nicking" of whole PA, is responsible for delivering the toxin's catalytic fragments (LF and EF) to the target cell's cytosol. In planar bilayer membranes, trypsin-nicked PA makes cation-selective voltage-gated channels with a pore diameter of $\geq$12 Å. The channels are presumed to be heptameric "mushrooms", with an extracellular "cap" region and a membrane-inserted, β-barrel "stem". Although the crystal structure of the water-soluble monomeric form has been resolved to 2.1 Å and that of the heptameric "prepore" to 4.5 Å, the structure for the membrane-bound channel (pore) has not been determined. We have engineered mutant channels that are cysteine-substituted in residues in the putative β-barrel, and identified the residues lining the channel lumen by their accessibility to a water-soluble sulfhydryl-specific reagent. The reaction with lumen-exposed cysteinyl side chains causes a drop in channel conductance, which we used to map the residues that line the pore. Our results indicate that the β-barrel structure extends beyond the bilayer and involves residues that are buried in the monomer. The implication is that major rearrangement of domains in the prepore cap region is required for membrane insertion of the β-barrel stem.

The toxin produced by *Bacillus anthracis* is composed of three proteins (EF, LF, and PA),[1] which act in binary and tertiary combinations to produce the clinical symptoms of anthrax (*1*). EF and LF have enzymatic functions; they both require PA to achieve their biological effects (*2*, *3*). Because EF and LF have cytosolic substrates, the challenge for PA is to dock onto target cells and to ferry its cargo (EF or LF) into the cytosol. This translocator−effector scheme is common to many toxins and has been defined as the A-B family, of which anthrax is a member (for general reviews of anthrax toxin, see refs *4* and *5*).

Monomeric PA is a cysteineless 83 kDa protein (*6*). It forms channels in planar bilayers and heptameric pores on cell membranes when the N-terminal 20 kDa segment is cleaved off (*7*) and the 63 kDa moiety (PA_{63}) experiences low pH (*8*, *9*). In vivo intoxication involves several steps: binding to the plasmalemma (*10*−*12*), protease cleavage (*13*), oligomerization (*14*), endocytosis of membrane-bound PA_{63} (*15*), and acidification of the endosome (*1*); PA_{63} then shuttles bound EF or LF across the endosomal membrane (*16*, *17*), presumably forming a pore in the process. On mammalian cells, a receptor is involved in the binding and oligomerization steps (*10*), but does not appear to be absolutely required; in artificial bilayers, excellent channel activity is obtained under mildly acidic conditions (*9*). The channels are voltage-gated and cation-selective, with a single-channel conductance of ~100 pS in 100 mM KCl (*18*). Sizing experiments indicate a minimum pore diameter of 12 Å and a binding site for the blocker, tetrabutylammonium (TBA) ion (*19*). As is the case with other pore-forming A-B toxins, it is not clear whether the pore lumen is the translocation pathway or is in any way required for enzyme delivery. An understanding of its architecture could be key to settling this mystery.

The primary structure of PA does not immediately suggest possibilities. There are no hydrophobic stretches which could serve as potential membrane-spanning regions. In the absence of a definitive crystal structure of the PA_{63} channel, a hypothetical structure has been proposed on the basis of the crystal structures of (1) the heptameric "prepore" (*20*) and (2) the heptameric, mushroom-shaped channel of *Staphylococcus aureus* α-hemolysin (i.e., "cap" and "stem" regions; see Figure 1A) (*21*). Of particular interest is the amphipathic transmembrane hairpin loop of the α-toxin protomer, each of which contributes two strands to the 14-stranded β-barrel stem (Figure 1B) (*21*). In the PA_{63} channel model, formation of a similar β-barrel requires that the analogous, but disordered, amphipathic $2\beta_2-2\beta_3$ loop peel away from the prepore cap and insert itself as a β-pleated sheet within the membrane (Figure 2). Such a rearrangement disrupts hydrogen bonds between underlying β-strands in domain 2 ($2\beta_1-2\beta_4$), which form a stable Greek-key motif (Figure 2) (*20*).

[†] This work was supported by National Institutes of Health Grants T-32-GM07288 (S.N.), AI-22021 (R.J.C.), and GM-29210 (A.F.).

[‡] Department of Neuroscience, Albert Einstein College of Medicine.

[§] Harvard Medical School.

[||] Department of Physiology and Biophysics, Albert Einstein College of Medicine.

[1] Abbreviations: PA, protective antigen; nPA, nicked PA; PA_{63}, C-terminal 63 kDa moiety resulting from nicked PA; EF, edema factor; LF, lethal factor; SCAM, substituted cysteine-accessibility mutagenesis; MTS-ET, methanethiosulfonate ethyltrimethylammonium; DTT, dithiothreitol; TCEP, tris(2-carboxyethyl)phosphine; BLM, black lipid membrane; cis compartment, side to which toxin is added; trans compartment, opposite side, held at virtual ground; TBA, tetrabutylammonium.

10.1021/bi0119518 CCC: $22.00
Published on Web 01/11/2002

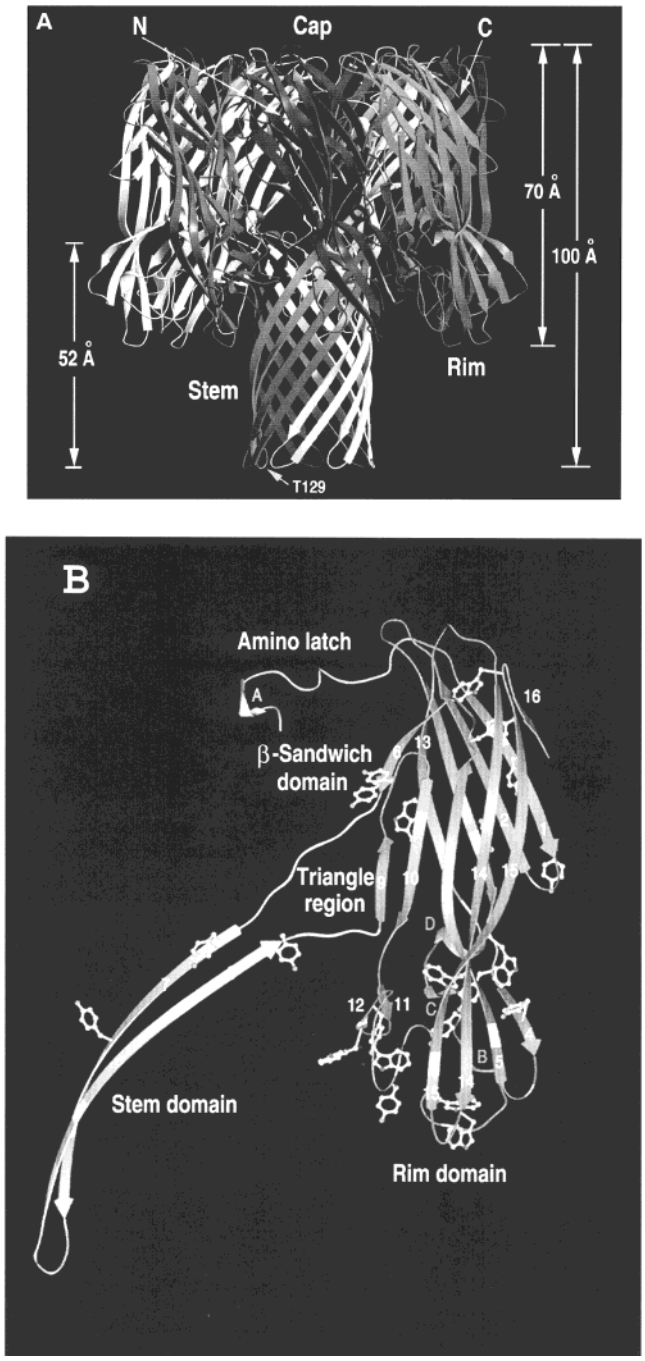

FIGURE 1: α-Hemolysin structure. (A) Ribbon representations of the heptameric channel. (B) Ribbon diagram of an isolated protomer, with β-strands numbered consecutively (from ref *21*).

The energetics of this transformation are presumably made favorable by (1) acidification of the endosome, which may protonate histidines in the loop and key, (2) reformation of hydrogen bonds in the β-sheet, and (3) repartitioning of charged and uncharged side chains of the $2\beta_2-2\beta_3$ loop into hydrophilic (aqueous) and hydrophobic (lipid) environments, respectively (*20*).

Benson et al. (*22*) confirmed the β-hairpin structure of the $2\beta_2-2\beta_3$ loop in the transmembrane domain of the PA_{63} channel. Using a technique fondly known as SCAM (*23*), they serially generated cysteine mutations in the $2\beta_2-2\beta_3$ loop and probed the mutant channels with the small (6 Å), thiolate-specific (*24*), membrane-impermeant (*25*) reagent MTS-ET.

Reaction of lumen-exposed sulfhydryl groups with the positively charged MTS reagent caused a drop in channel conductance, presumably through steric and electrostatic effects. Residues in the $2\beta_2-2\beta_3$ loop exhibited an alternating pattern of susceptibility to MTS-ET, except for two consecutive residues in the middle, consistent with a β-hairpin loop at the water−lipid interface (see Figure 4). On the single-channel level, these reactions were seen as small, stepwise drops in current, which staggered back up again upon addition of DTT (*22*).

The results of this study extend the span of the β-barrel, possibly to amino acids 285−340. Indeed, lumen-exposed side chains have been identified as far as residues 276 and 351. These residues lie between $2\beta_1$ and $2\beta_4$ and are somewhat buried in the protomers of the PA prepore. Some movement of the occluding domains is required to expose them. Construction of the barrel thus necessitates a major rearrangement of domains in the prepore. Recent studies (*26*) support the idea that major movement of domains in the cap region is associated with PA_{63} channel formation.

MATERIALS AND METHODS

Bacterial Strains and Plasmids. The plasmid used as the template in PCR was a pET22b$^+$-PA construct with a wild-type PA containing a C-terminal histidine tag cloned into the Bam*HI*−Xho*I* site. The pET22b$^+$ (Novagen) plasmid encodes a signal peptide which directs expressed proteins to the periplasm.

The transformation cell strain was a supercompetent XL1-Blue cell line provided by Stratagene in its Quick-Change kit. The expression strain was the heat-shock-competent BL21(DE3) strain. BL21 cells were transformed according to standard protocols (*27*).

All cultures were grown in Luria-Bertani (LB) broth and ampicillin (100 μg/mL).

Generation of Mutants. PA cysteine mutants were generated using PCR, following the protocol in Stratagene's Quick-Change Site-Directed Mutagenesis Kit. Mutagenic oligonucleotides were provided by Gibco. The correct sequence (including the presence of mutation) was verified via automated sequencing of amplified plasmid DNA in an approximately 700 bp stretch encompassing the mutation.

Preparation of Proteins. Overnight cultures were diluted 1:50 in LB broth and grown for 3 h (with rotary shaking at 37 °C); protein expression was then induced with 1 mM isopropyl β-D-thiogalactopyranoside (IPTG) (Labscientific, Inc.) at 30 °C for an additional 3 h. The pelleted cells were resuspended in 20% glucose (4 mL/g of wet pellet), lysozyme (0.1 mg/mL) (Sigma), and EDTA (5 mM). The suspension was incubated on ice for approximately 35 min, after which $MgCl_2$ (20 mM) was added. The cells were centrifuged again (20 min at 10K rpm in a Sorvall GSA rotor), and the supernatant was dialyzed against binding buffer [150 mM NaCl, 20 mM Tris-HCl, 5 mM imidazole, and 1 mM EDTA (pH 7.9)]. All samples were purified on Novagen His-Bind Nickel columns according to their protocol, and PA-containing fractions (approximately 0.2−1 mg/mL) were dialyzed into 20 mM Tris, 150 mM NaCl, 5 mM DTT, and 1 mM EDTA (pH 8). (The protein purity in each fraction was assessed by Coomassie blue staining of SDS−PAGE gels.) Prior to the experiments, samples were nicked with

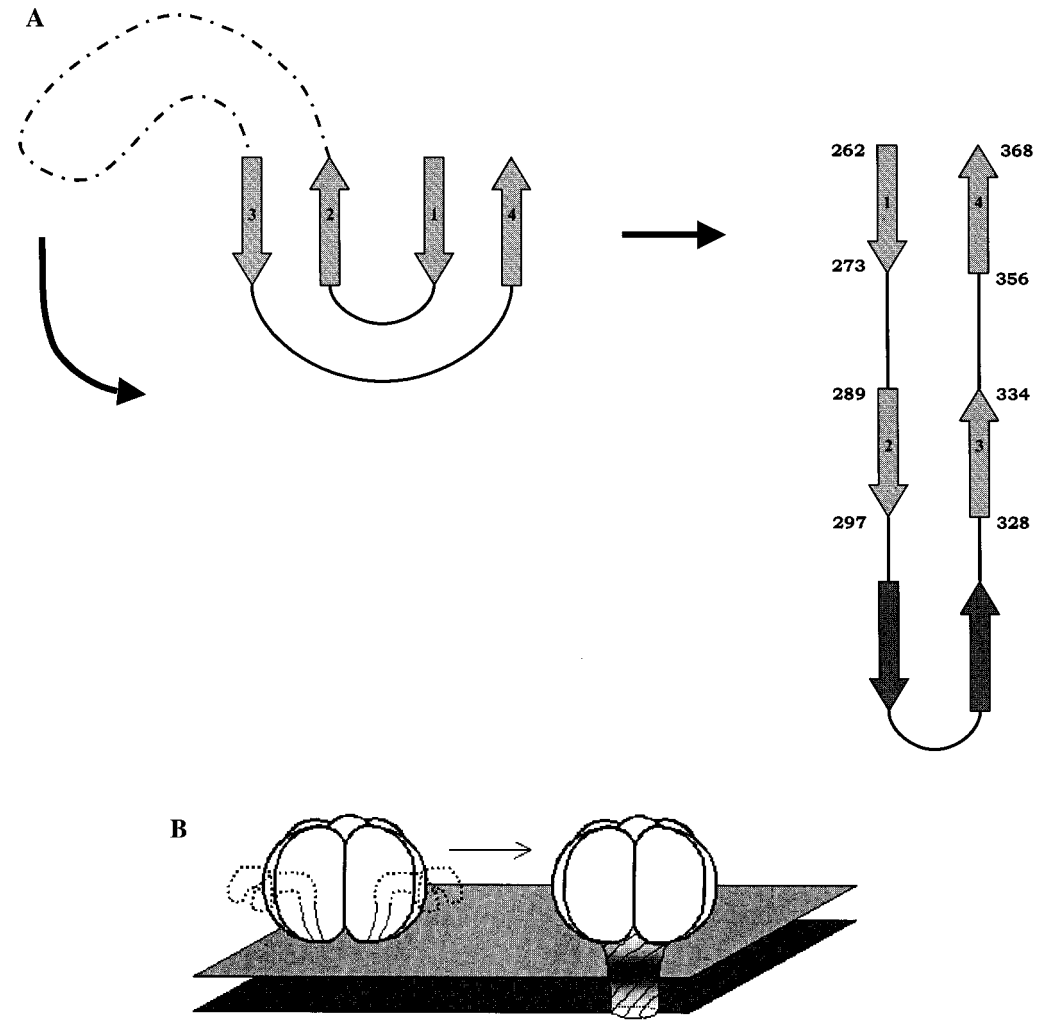

FIGURE 2: Model of membrane insertion of PA_{63}. (A) Unfolding of the Greek-key motif (strands $2\beta_1-2\beta_4$) to form a β-hairpin. (B) Association of the seven β-hairpins in the PA_{63} heptamer to form a 14-stranded, membrane-inserted β-barrel (adapted from ref *20*).

trypsin (1 μg/mL) (Worthington) for 5 min at 37 °C, and further nicking was blocked with the soybean trypsin inhibitor (10 μg/mL) (Worthington). (Nicking was confirmed by a gel shift of samples from 83 to 63 kDa on SDS−PAGE.) Finally, DTT was added to a concentration of 20 mM, and the samples were allowed to sit at room temperature for approximately 30 min. All samples were stored at 4 °C between preparation and experimentation.

Bilayer Experiments. Bilayers were formed at room temperature by the brush technique of Mueller et al. (*28*) across a 0.5 mm diameter hole in a Teflon partition separating two continuously stirred 3 mL Lucite compartments containing symmetric solutions of 100 mM KCl, 10 mM DMG (dimethylglutarate), and 1 mM EDTA (pH 6.6). Bridges containing 3 M KCl in 3% agar connected the solutions to Ag/AgCl electrodes in saturated KCl baths. The painted lipid, 3% diphytanoylphosphatidylcholine (Avanti Polar Lipids, Inc.) in decane, thinned to secondary black before addition of trypsin-nicked PA (nPA) to the cis compartment. (The cis compartment is that to which proteins were added; the opposite, the trans compartment, was held at virtual ground.) Protein and DTT concentrations in each experiment varied between 0.3 and 3 μg/mL and between 5 and 80 μM, respectively. With the membrane voltage clamped at 20 mV, the nPA-induced conductance ($g = I/V_{cis}$) was allowed to plateau over several minutes before addition of MTS-ET (Toronto Research Chemicals) to the trans compartment (final concentration of 20 μg/mL). (This concentration of MTS-ET had no effect on conductances induced by wild-type nPA.) The response of mutant channels occurred, if at all, within seconds of addition of MTS-ET. The MTS-ET-induced conductance drop, which varied from 50 to 90%, was reversed with millimolar concentrations of DTT or TCEP (cis or trans). Some mutants were additionally tested, following addition of MTS-ET, for response to the channel blocker TBA (13−15 μM cis, and/or 400−600 μM trans). A Narco Physiographic chart recorder duly noted the current (filtered at 10 Hz).

RESULTS

We generated cysteine mutants of PA from residues in the stretch from $2\beta_1$ to $2\beta_4$ (exclusive of the $2\beta_2-2\beta_3$ loop) and tested the response of mutant nPA channels to the cysteine-specific reagent MTS-ET on BLMs. In general, we obtained good activity from most of the mutants, the voltage-gated behavior of which was similar to that of the wild type.

In each experiment, nPA was added to a continuously stirred compartment (cis) of a bipartite chamber to a final concentration of ~0.3−3 μg/mL and allowed to develop an essentially constant conductance before addition, at 20 mV, of trans MTS-ET (20 μg/mL). The final DTT concentration

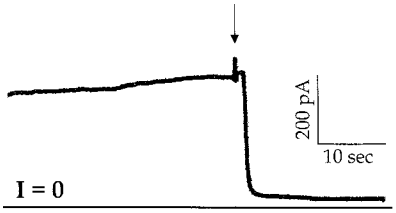

FIGURE 3: Effect of MTS-ET on channels formed by N329C. Approximately 2.5 min prior to the start of the record, trypsin-nicked PA N329C was added to the cis compartment to a final concentration of ~100 ng/mL. The conductance increased continuously over time and was still rising when MTS-ET was added to the trans compartment (arrow) to a final concentration of 20 μg/mL. The current is seen to decrease within seconds to less than one-tenth of its original value. Throughout the experiment, the voltage was held at 20 mV.

(see Materials and Methods) was approximately 20 μM. The steady-state conductance represented the conductance of hundreds of channels. The MTS-ET effect (if it occurred) could be observed within seconds after addition (e.g., Figure 3) and could be reversed upon addition of reductant (e.g., DTT).

The responses of the mutants, along with previous results from Benson et al. (*22*), are summarized in Figure 4. In the N-terminal strand, reactivity alternates from residue 276 to 312, which is consistent with β-sheet topology, but with an "interruption" of the three residues between residues 281 and 285; in the other strand, the pattern continues from residue 315 to 351 with an exception in residue 341. For a few residues (indicated in the figure), we were unable, for various reasons,[2] to perform bilayer experiments.

Several residues were also probed with TBA after reaction with MTS-ET (data not shown). Previous studies had demonstrated a voltage-dependent block of PA_{63} channels with TBA, leading to a single-well, two-barrier model for TBA binding within the channel lumen (*18*). At 20 mV, an approximately 40-fold higher trans concentration was required to produce the same effect as a given cis concentration (*19*). Benson et al. (*2*) had demonstrated that even after S325C channels had reacted with MTS-ET, subsequent addition of 15 μM TBA to the cis side produced its usual 3.5-fold fall in conductance, whereas the MTS-ET reaction prevented 500 μM trans TBA from producing its usual 2-fold fall in conductance. This suggested that the TBA binding site is cis relative to the $2\beta_2-2\beta_3$ loop (which ends at S325), the rationale being that ethyltrimethylammonium ions bound within the channel lumen act to electrostatically blockade the TBA-binding site, if the site lies downstream of the derivatized region. Thus, both the accessibility of the binding site to cis TBA and its inaccessibility to trans TBA are consistent with a location of the site that is cis relative to residue 325. We also observed the cis TBA response, following reaction with MTS-ET, of T349C channels, but essentially no effect of trans TBA (600 μm), suggesting that the TBA binding site is somewhere in the cap.

DISCUSSION

Crossing the membrane barrier of the cell is the first order of business for intracellularly acting toxins and presents a

[2] These reasons included failure to express the mutant, degradation of PA_{63} during trypsin nicking, and failure to form channels in ostensibly properly nicked PA.

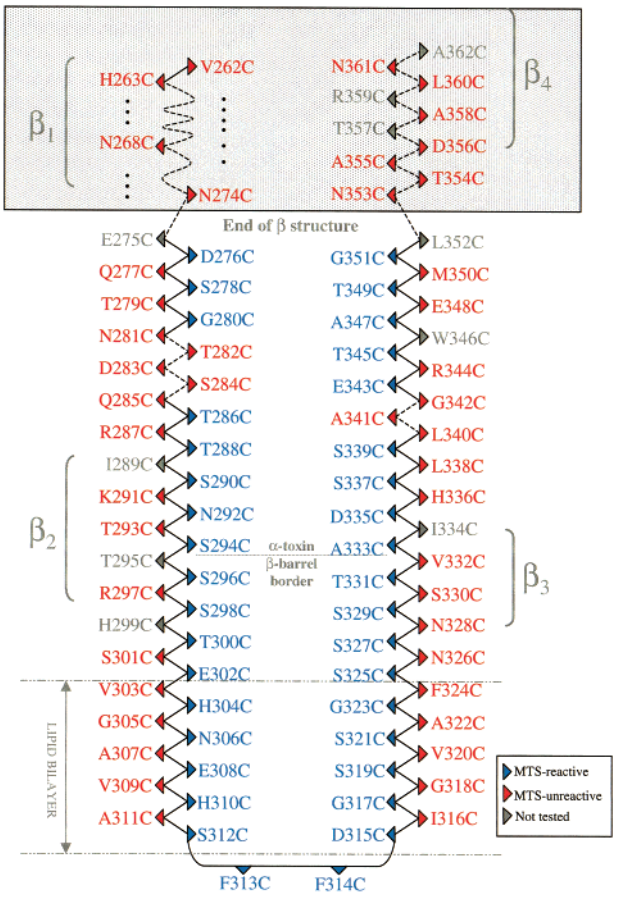

FIGURE 4: Susceptibility of cysteine-substituted residues in domain 2 to MTS-ET. Residues in blue reacted; those in red did not. Gray residues were not tested. The stretch from E302 to S325 constitutes the membrane-spanning region (the $2\beta_2-2\beta_3$ loop), which was previously probed by Benson et al. (*22*). Solid lines represent peptide linkages that are consistent with β-sheet topology; dashed lines represent those that are not. (Note the discontinuities of β-sheet topology in T282−S284 and A341.) The β-strands ($2\beta_1-2\beta_4$) of the monomer are also illustrated as landmarks. The stretch encompassing T295−V332 corresponds to the span of the β-barrel in α-toxin, as indicated by a dotted line.

nontrivial challenge. Once at the cell surface, the hydrophilic molecule must somehow traverse the hydrophobic lipid. Such a dramatic transition in its milieu requires a significant conformational change of the toxin, which must then subsequently act on a cytosolic substrate. In the A-B toxins, translocation and catalytic (enzyme) functions are assigned to different peptide domains or, in the case of anthrax, to discrete proteins; enzyme trafficking is often accompanied by pore formation. Whether the pore lumen represents the conduit for the hydrophilic enzymatic domain or is merely a membrane-insertion epiphenomenon is unknown.

In anthrax toxin, the pore-forming domain, PA_{63}, makes stable homoheptameric channels in cells, liposomes, and planar bilayers (*14*, *20*). Earlier work exploited cysteine biochemistry in identifying and mapping the pore-lining residues of the membrane-spanning segment of PA_{63}. Benson et al. (*22*) used a conductance drop as a measure of side chain accessibility of cysteines in mutant channels to a sulfhydryl-specific reagent, MTS-ET. The alternating pattern of reactivity that emerged was consistent with a β-hairpin structure, which, when integrated over seven protomers, was suggestive of a β-barrel spanning the membrane. In their

analysis, they were guided by the crystal structures of the 83 kDa PA monomer, the oligomeric PA_{63} prepore, and the pore of *S. aureus* α-hemolysin, to which PA bears a striking resemblance (*20*, *21*). Both toxins are composed almost exclusively of β-strands; both form homoheptamers following or preceding membrane binding, and then undergo a poorly understood prepore-to-pore conversion that is dependent on low pH (*8*, *29*) and confers SDS resistance upon the aggregate (*29*, *30*). They form voltage-gated channels of comparable size (12−14 Å minimum diameter) and conductance (100 pS in 100 mM KCl) (*31*, *32*). Most specifically, both molecules have a central amphipathic domain, the primary structure of which resembles the alternating hydrophilic/hydrophobic motif also found in the membrane-spanning hairpins of β-barrel porins (*33*, *34*), and thus suggests a β-pleated sheet inserted into a lipid−water interface. Indeed, in the α-hemolysin channel, the β-hairpins from each protomer combine to form a water-filled β-barrel stem traversing the bilayer (see Figure 1). In the PA_{63} prepore, the amphipathic segment (the $2\beta_2-2\beta_3$ loop) exists in a disordered state on the exterior of its midsection (see Figure 2). Movement of this loop into the bilayer requires unfolding of the β-sheets underlying it, which is probably facilitated by protonation of histidines (*20*). This rearrangement disrupts the structure of domain 2, and perhaps of the prepore as a whole. Moreover, it implies participation of segments of the polypeptide contiguous to the $2\beta_2-2\beta_3$ loop in the formation of the barrel, which would potentially make the stem domain longer than the loop.

In α-toxin, the protomer stem domain is composed of 39 residues, the middle 24 of which span the membrane (*21*). As a consequence of the tilt of the barrel, the stem extends 24 Å beyond the bilayer, making a 180° twist around the barrel axis (*21*). It is joined to the cap domain by a triangle region of β-pleated conformation (Figure 1B). Each strand of the triangle region forms hydrogen bonds with triangle strands on adjacent protomers and mediates protomer−protomer contact. This region is flanked at both the carboxy and amino ends by β-sheets in the cap domain. Thus, the involvement of β-sheet topology in the luminal surface of the channel is extensive and is not restricted to the stem.

To further explore the extent to which polypeptides contiguous to the $2\beta_2-2\beta_3$ loop contribute to the PA_{63} channel stem, we employed the same derivatization methods as Benson et al. (*22*) with cysteine mutants in the segments upstream and downstream of the β-hairpin. In contrast to the $2\beta_2-2\beta_3$ loop, these regions consist almost entirely of hydrophilic amino acids and do not immediately hint at β-sheet structure (*6*). Nevertheless, we found that, in the stretches from D276 to E302 and from S325 to G351, mutant channel sensitivity to MTS-ET alternates, consistent with a β-pleated conformation of these residues (Figure 4). However, there are two notable exceptions (which we will call "bulges"): the first is A341C in the C-terminal strand, and the second is the stretch of T282−S284 in the N-terminal strand. (Interestingly, the pattern resumes beyond these residues in register; i.e., even residues on one limb, and odd residues on the other, are susceptible to MTS-ET.)

The pattern of MTS-ET reactivity appears to extend the β-barrel beyond the limit of the bilayer and raises intriguing possibilities about the relationship of PA to other known β-barrel pores, particularly to α-hemolysin. Unfortunately, due to the lack of a more definitive structure, it is impossible to assign hydrogen bonding patterns and thus establish which residues are paired. Nevertheless, we can, with some confidence, place aromatic residues F324 and F313/F314 at opposite interfacial boundaries of the bilayer. Other pore-forming proteins, such as OmpA, *Escherichia coli* maltoporin, and the *Rhodobacter capsulatus* porin, also have similar aromatic "belts" (*34*, *35*). [However, in α-hemolysin, both bands (Y118 and F120) are located at the extracellular boundary (*34*).] Even more compellingly, the alternating pattern of hydrophilicity and hydrophobicity ends in the $2\beta_2-2\beta_3$ loop. Given that F324/S325 and E302/V303 can be placed at the lipid phosphate−fatty acid interface, it is likely that PA_{63} residues line up within one to two places from their positions in Figure 4 and that the bulge regions are skewed with respect to each other.

There are at least three interpretations of our results. The first is that the stem domain continues to the vicinity of T286−S339, where it is disrupted by two β-bulges. β-Bulges introduce kinks and twists in β-sheets (*36*, *37*) that are incompatible with β-barrel structure. The remaining stretches could potentially join this "kinky" barrel to the cap like the triangle region of α-toxin (see Figure 1B), or could themselves be part of the cap domain.

Alternatively, the bulge could represent the triangle region, the difference (from α-toxin) being that its side chains are facing away from the lumen. The remaining amino acids would thus lie in β-sheets in the cap.

In both these scenarios, the PA_{63} stem domain is considerably longer than the α-toxin stem domain and extends farther from the bilayer, 41 Å instead of 24 Å. [Placement of the aromatic belts suggests that the PA_{63} barrel has the same tilt as α-hemolysin (*38*), and allows us to estimate distances.]

The third interpretation is that the β-strands separate around V332 and T295 (corresponding to the α-toxin stem domain border; see Figure 4) and the remaining alternate residues represent the triangle region. The bulge stretch could just be an unexposed loop between the stem and cap and the remaining amino acids β-sheets within the cap. This scenario infers from our data that the PA_{63} heptamer has an ultrastructure similar to that of α-toxin.

Note that none of these explanations can adequately account for the fact that the discontinuous β-sheets on each strand are in register. It is possible that residues 282, 284, and 341 are anomalous and, even though they face the lumen, either do not react with MTS or do not display a conductance drop when they do react with MTS. Although there is no reason a priori to suspect this, it is theoretically possible.

K397 and D425 face the lumen in the crystal structure of the prepore. Single-alanine substitution of both residues obliterates pore-forming and translocation activities in CHO-K1 cells by arresting the oligomers in an SDS-sensitive stage (*26*), suggesting that these amino acids are critically involved in the conformational changes accompanying prepore-to-pore conversion. Since they are far removed from the $2\beta_2-2\beta_3$ loop in the prepore crystal structure, and in fact lie outside domain 2, their implication in pore formation means that a major metamorphosis of the prepore takes place upon insertion of the loop into the bilayer, in support of our results.

And finally, we were unable to locate the elusive TBA binding site, as it appears to lie cis relative to all domain 2 residues we tested, including T349.

ACKNOWLEDGMENT

We thank Dr. Rachel Legmann for T298C and T300C, Dr. K. Joon Oh for the purification protocol, Dr. Bret Sellman for T473C, and Dr. D. Borden Lacy for help in preparing the figures.

REFERENCES

1. Friedlander, A. M. (1986) *J. Biol. Chem. 261*, 7123−7126.
2. Molnar, D. M., and Altenbern, R. A. (1963) *Soc. Exp. Biol. Med. 114*, 294−297.
3. Leppla, S. H. (1982) *Proc. Natl. Acad. Sci. U.S.A. 79*, 3162−3166.
4. Duesbery, N. S., and Vande Woude, G. F. (1999) *Cell. Mol. Life Sci. 55*, 1599−1609.
5. Leppla, S. H., Ivins, B. E., and Ezzell, J. W. (1985) *Anthrax Toxin*, Vol. 1985, American Society for Microbiology, Washington, DC.
6. Welkos, S. L., Lowe, J. R., Eden-McCutchan, F., Vodkin, M., Leppla, S. H., and Schmidt, J. J. (1988) *Gene 69*, 287−300.
7. Leppla, S. H., Friedlander, A. M., and Cora, E. M. (1988) in *Bacterial Protein Toxins* (Fehrenbach, F. e. a., Ed.) pp 111−112, Gustav Fischer, Stuttgart, Germany.
8. Milne, J. C., and Collier, R. J. (1993) *Mol. Microbiol. 10*, 647−653.
9. Blaustein, R. O., Koehler, T. M., Collier, R. J., and Finkelstein, A. (1989) *Proc. Natl. Acad. Sci. U.S.A. 86*, 2209−2213.
10. Escuyer, V., and Collier, R. J. (1991) *Infect. Immun. 59*, 3381−3386.
11. Singh, Y., Klimpel, K. R., Quinn, C. P., Chaudhary, V. K., and Leppla, S. H. (1991) *J. Biol. Chem. 266*, 15493−15497.
12. Novak, J. M., Stein, M. P., Little, S. F., Leppla, S. H., and Friedlander, A. M. (1992) *J. Biol. Chem. 267*, 17186−17193.
13. Klimpel, K. R., Molloy, S. S., Thomas, G., and Leppla, S. H. (1992) *Proc. Natl. Acad. Sci. U.S.A. 89*, 10277−10281.
14. Milne, J. C., Furlong, D., Hanna, P. C., Wall, J. S., and Collier, R. J. (1994) *J. Biol. Chem. 269*, 20607−20612.
15. Gordon, V. M., Leppla, S. H., and Hewlett, E. L. (1988) *Infect. Immun. 56*, 1066−1069.
16. Little, S. F., Novak, J. M., Lowe, J. R., Leppla, S. H., Singh, Y., Klimpel, K. R., Lidgerding, B. C., and Friedlander, A. M. (1996) *Microbiology 142*, 707−715.
17. Singh, Y., Klimpel, K. R., Goel, S., Swain, P. K., and Leppla, S. H. (1999) *Infect. Immun. 67*, 1853−1859.
18. Blaustein, R. O., Lea, E. J., and Finkelstein, A. (1990) *J. Gen. Physiol. 96*, 921−942.
19. Blaustein, R. O., and Finkelstein, A. (1990) *J. Gen. Physiol. 96*, 905−919.
20. Petosa, C., Collier, R. J., Klimpel, K. R., Leppla, S. H., and Liddington, R. C. (1997) *Nature 385*, 833−838.
21. Song, L., Hobaugh, M. R., Shustak, C., Cheley, S., Bayley, H., and Gouaux, J. E. (1996) *Science 274*, 1859−1866.
22. Benson, E. L., Huynh, P. D., Finkelstein, A., and Collier, R. J. (1998) *Biochemistry 37*, 3941−3948.
23. Karlin, A., and Akabas, M. H. (1998) *Methods Enzymol. 293*, 123−145.
24. Akabas, M. H., Kaufmann, C., Archdeacon, P., and Karlin, A. (1994) *Neuron 13*, 919−927.
25. Holmgren, M., Liu, Y., Xu, Y., and Yellen, G. (1996) *Neuropharmacology 35*, 797−804.
26. Sellman, B. R., Nassi, S., and Collier, R. J. (2001) *J. Biol. Chem. 276*, 8371−8376.
27. Sambrook, J., Fritsch, E. F., and Maniatis, T. (1989) *Molecular cloning: a laboratory manual*, 2nd ed., Cold Spring Harbor Laboratory Press, Plainview, NY.
28. Mueller, P. D., Rudin, H. T., Tien, H. T., and Wescott, W. C. (1963) *J. Phys. Chem. 67*, 534−535.
29. Miller, C. J., Elliott, J. L., and Collier, R. J. (1999) *Biochemistry 38*, 10432−10441.
30. Valeva, A., Palmer, M., and Bhakdi, S. (1997) *Biochemistry 36*, 13298−13304.
31. Menestrina, G. (1986) *J. Membr. Biol. 90*, 177−190.
32. Finkelstein, A. (1994) *Toxicology 87*, 29−41.
33. Koebnik, R., Locher, K. P., and Van Gelder, P. (2000) *Mol. Microbiol. 37*, 239−253.
34. Gouaux, E. (1998) *Nat. Struct. Biol. 5*, 931−932.
35. Schirmer, T. (1998) *J. Struct. Biol. 121*, 101−109.
36. Richardson, J. S., Getzoff, E. D., and Richardson, D. C. (1978) *Proc. Natl. Acad. Sci. U.S.A. 75*, 2574−2578.
37. Chan, A. W., Hutchinson, E. G., Harris, D., and Thornton, J. M. (1993) *Protein Sci. 2*, 1574−1590.
38. Benson, E. (1998) in *Department of Microbiology & Molecular Genetics*, pp 191, Harvard University, Cambridge, MA.

BI0119518